

# Gapless spin liquid state of the spin- $\frac{1}{2}$ honeycomb antiferromagnetic $\Gamma$ model

Qiang Luo,<sup>1</sup> Jize Zhao,<sup>2,\*</sup> and Xiaoqun Wang<sup>3,4,†</sup>

<sup>1</sup>*Department of Physics, Renmin University of China, Beijing 100872, China*

<sup>2</sup>*School of Physical Science and Technology & Key Laboratory for Magnetism and Magnetic Materials of the MoE, Lanzhou University, Lanzhou 730000, China*

<sup>3</sup>*Key Laboratory of Artificial Structures and Quantum Control (Ministry of Education), School of Physics and Astronomy, Tsung-Dao Lee Institute, Shanghai Jiao Tong University, Shanghai 200240, China*

<sup>4</sup>*Beijing Computational Science Research Center, Beijing 100084, China*

(Dated: March 23, 2022)

Recently, what on earth is the faithful ground state of the spin-1/2 honeycomb  $\Gamma$  antiferromagnet (HCGA) has caused drastic debates. To eliminate such controversy, we propose a choreographed model by introducing a bond-modulated Heisenberg interaction ( $J$ ) in addition to the  $\Gamma$  term. By varying the angular parameter  $\vartheta = \text{atan}(\Gamma/J)$  in  $[0, \pi]$ , we demonstrate that the classical ground state of this model changes from a zigzag order to a stripy order, through a mixed phase and a noncoplanar phase. In the quantum case, we resort to the density-matrix renormalization group method to calculate the ground-state properties and find a gapless quantum spin liquid (QSL) phase when  $0.50 \leq \vartheta/\pi \lesssim 0.66(1)$ . It turns out that the ground state of the HCGA, corresponding to  $\vartheta = \pi/2$  in the phase diagram, belongs to the gapless QSL phase. Our findings are further verified by scanning the variable parameter  $\vartheta$  on a long but finite cylinder.

*Introduction.* – The ongoing search for exotic magnetic states in highly frustrated antiferromagnets [1–4] has been extended to a new class of correlated materials with two-dimensional (2D) honeycomb lattice[5–7] and its high-dimensional variants[8]. It is suggested[9] that the bond-dependent magnetic interactions[10] could be realized in the strongly spin-orbit coupled Mott insulators within the aforementioned lattice geometry. The Kitaev interaction[11], in particular, is such an anisotropic one, and the ground state of the corresponding model is the Kitaev quantum spin liquid (QSL) which hosts fractionalized Majorana fermions and flux excitations. Physical realization of the Kitaev interaction in real materials was first proposed in iridates [12–14], and then turned toward ruthenium trichloride  $\alpha$ -RuCl<sub>3</sub> in which Ru<sup>3+</sup> ions are arranged in a honeycomb lattice and carry effective spin-1/2 particles [5–7]. Although  $\alpha$ -RuCl<sub>3</sub> displays long-range zigzag magnetic order at low temperature [15–21], it has been argued to be proximate to the Kitaev QSL because of its broad continuum of magnetic excitations identified in Raman scattering[22, 23] and inelastic neutron scattering[6, 7, 24–26].

Despite a flood of attentions have been attracted by the Kitaev interaction [27–37], it is undeniable that a sizable antiferromagnetic (AFM) off-diagonal symmetric  $\Gamma$  interaction is also of vital importance to  $\alpha$ -RuCl<sub>3</sub> as well as other materials (see ref. [38] and references therein) and thus should be considered on an equal footing[39–45]. Interestingly, it is shown that the  $\Gamma$  interaction itself may be responsible for the strongly anisotropic responses to the magnetic field observed in  $\alpha$ -RuCl<sub>3</sub>[38, 46]. The two models severally show somewhat similarity on the temperature dependence of the specific heat where two pronounced peaks are observed at  $T_l$  and  $T_h$  and a plateau in the thermal entropy could be spotted in between[47, 49].

In contrast to the Kitaev model on the honeycomb lattice, the pure  $\Gamma$  model is not exactly solvable but the phenomenal resemblance and a highly degenerate manifold in its classical ground state[48] render people to believe that its quantum ground state may also be a QSL[49]. The quantum order-by-disorder mechanism, however, suggests that while the system remains highly frustrated even at  $T_l \lesssim 0.03\Gamma$ [49], it will eventually order at a energy scale that is much lower than  $T_l$ [48]. As a result, in the numerical calculations considerable attentions should be paid to this issue due to the formidable battle among various possible competing states. Unfortunately, existing numerical works have already led to contradictory conclusions on the nature of the ground state of the honeycomb  $\Gamma$  antiferromagnet (HCGA). On one hand, the parallel works by exact diagonalization of small cluster with 24 sites in total[50] and density-matrix renormalization group (DMRG) study of narrow infinite cylinder with a three-unit-cell circumference[51] both claim that the ground state is a magnetically disordered phase. A scenario of QSL phase with a hidden flux long-range order was unwittingly argued to be a strong candidate for low-temperature state[52]. On the other hand, recent variational Monte Carlo simulation argues that it is preferably a zigzag order[53].

In this letter, we employ the 2D DMRG method[54, 55] to explore the nature of the spin-1/2 HCGA. We demonstrate that the quantum ground state of this model is a gapless QSL. We arrive at this conclusion by studying a choreographed model which consists of the  $\Gamma$  term and bond-modulated Heisenberg interaction. We find a QSL phase with vanishing energy gap sandwiched between two magnetically ordered states. Remarkably, we show that the HCGA locates at the leftmost boundary of this gapless QSL phase which is separate from a zigzag phase by

a first-order phase transition.

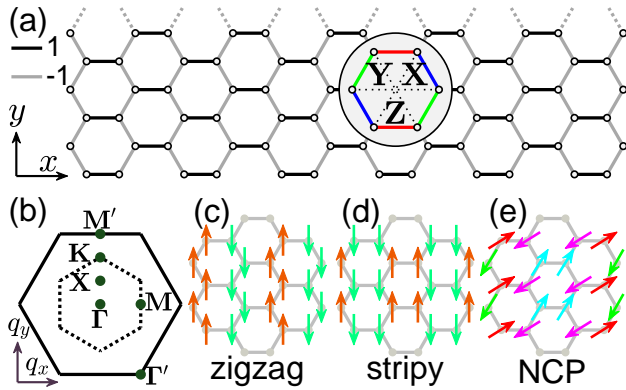


FIG. 1: (a) Illustration of an XC6 cylinder on a honeycomb lattice. The phase factor  $\eta_{ij}$  along the horizontal bonds (black) is  $+1$ , while it is  $-1$  for the bonds (gray) along the so-called zigzag direction. The inset zooms in one hexagon showing NN interaction of  $\mathbf{X}$  (blue),  $\mathbf{Y}$  (green), and  $\mathbf{Z}$  (red) bonds. (b) First and second Brillouin zones of a honeycomb lattice. (c) and (d) show two classical magnetically ordered states dubbed zigzag order and stripy order, respectively. The zigzag order can be described as ferromagnetic zigzag chains coupled antiferromagnetically. The stripe order, inversely, is formed by antiferromagnetic zigzag chains with ferromagnetic coupling. (e) A noncoplanar phase with a unit cell of  $4 \times 2$ .

*Model.* – The model is a nearest-neighbor (NN)  $\Gamma$  model with a bond-modulated Heisenberg term ( $J$ ). Its Hamiltonian is of the following form

$$\mathcal{H} = J \sum_{\langle ij \rangle} \eta_{ij} \mathbf{S}_i \cdot \mathbf{S}_j + \Gamma \sum_{\langle ij \rangle || \gamma} (S_i^\alpha S_j^\beta + S_i^\beta S_j^\alpha) \quad (1)$$

where  $S_i^\gamma$  ( $\gamma = x, y$ , and  $z$ ) is the  $\gamma$ -component of spin-1/2 operator at site  $i$ , and  $\alpha$  and  $\beta$  are the two other bonds on a honeycomb lattice. Throughout the following,  $J$  and  $\Gamma$  are parameterized using  $\vartheta$  so as to  $J = \bar{J} \cos \vartheta$  and  $\Gamma = \bar{J} \sin \vartheta$  ( $\bar{J} = 1$  is the energy unit hereafter).  $\vartheta \in [0, \pi]$  such that  $\Gamma \geq 0$  and  $J$  could be either ferromagnetic or antiferromagnetic. The phase factor  $\eta_{ij} = 1$  for the bond  $\langle ij \rangle$  along the horizontal direction and equals to  $-1$  otherwise (see Fig. 1(a)). We first unveil the classical phase diagram of Eq. (1) by the parallel tempering Monte Carlo (PTMC) method[56, 57]. After that we perform large-scale 2D DMRG simulations to study its quantum version. In the latter case, the cylindrical boundary condition (CBC) on XC $n$  clusters of  $L_x \times L_y$  with fixed aspect ratio  $L_x/L_y = 2$  is used unless stated otherwise. Here, XC $n$  means a cylinder where one set of hexagons' edges parallel to the  $x$  direction, and  $n$  ( $= L_y/a$ ) spins are weaved periodically along the circumferential zigzag columns[58, 59]. Due to the zigzag edge of the cylinders, we shall only consider even circumferences  $n$  ranging from 4 to 10 lattice spacing ( $a = 1$ ).  $N = L_x L_y$  is the total number of spins. We keep up to  $m = 3000$  states in our

simulations and perform about 12 sweeps so as to ensure that the typical truncation error is smaller than  $10^{-6}$ .

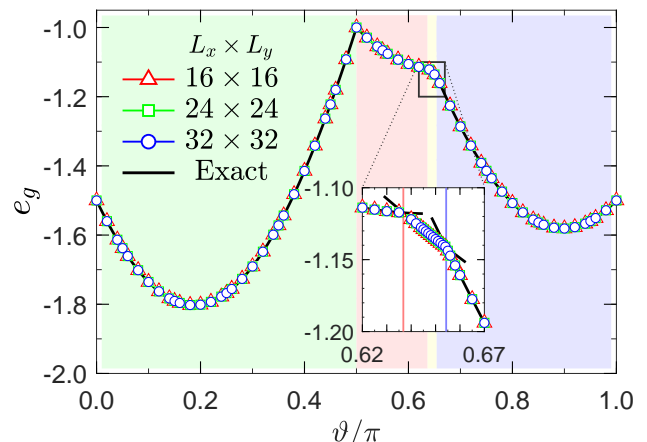


FIG. 2: The classical ground-state energy  $e_g$  obtained by PTMC on three XC clusters of  $16 \times 16$  (red triangle),  $24 \times 24$  (green square), and  $32 \times 32$  (blue circle). The solid black line represents the exact solution. Inset: Zoom in of the energy curves near the right-hand side transition point.

*Classical phase diagram.* – We firstly give a glance of the classical phase diagram before referring to the quantum effect. Classically, the ground states of the model (1) with  $\vartheta/\pi$  equaling to 0.0, 0.5, and 1.0, are zigzag order (see Fig. 1(c)), classical spin liquid with macroscopically degeneracy[48], and stripy order (see Fig. 1(d)), respectively. Due to the lack of  $C_6$  rotational symmetry in Eq. (1), the other two zigzag orders with different spin orientations are not equivalent to the one shown in Fig. 1(c) (see the Supplemental Material (SM) for detail[60]). In order to avoid confusion, we reserve the terminology of zigzag order for the spin pattern presented in Fig. 1(c), and call the other two as twining zigzag orders. Such a nomenclature also holds for the stripy order. Generally, whether there is a direct transition between the zigzag and stripy phases or not is unclear *a priori*. To untangle the mystery, we turn to the PTMC simulation to target the ground state[56, 57]. The simulation is performed on three XC clusters of  $16 \times 16$ ,  $24 \times 24$ , and  $32 \times 32$  under toroidal boundary condition. The final ground-state energy per site (*i.e.*, in unit of  $NS^2$ )  $e_g$  is shown in Fig. 2. It could be spotted that it is not a direct transition but undergoes an extensive intermediate region between the two ordered phases with energies  $e_g^{\text{zigzag}} = -(2\Gamma + 3J)/2$  and  $e_g^{\text{stripy}} = -(\Gamma - 3J)/2$ , respectively. The intermediate region is dominated by a so-called mixed phase in which the AFM order and the two twining zigzag orders are degenerate with energy  $e_g^{\text{mixed}} = -(2\Gamma - J)/2$ [60]. Therefore, the transition between the zigzag phase and mixed phase takes place exactly at  $\vartheta_{t,l}/\pi = 1/2$ . Interestingly, there is no direct transition between the mixed phase and the stripy phase expected to occur at  $\vartheta_{t,r}/\pi = 1 - \frac{1}{\pi} \text{atan} 2 \approx 0.6476$ .

Instead, an unexpected noncoplanar (NCP) phase appears in a rather narrow region (the window of  $\vartheta/\pi$  is less than 0.02, see inset of Fig. 2). Such a NCP phase can have many degenerate manifolds whose unit cells contain dozens of sites[60]. For the specific configuration shown in Fig. 1(e), its ordering wavevector is  $\mathbf{Q} = (\pi/3, 0)$  and its energy is  $e_g^{\text{NCP}} = -\sqrt{J^2 + \Gamma^2/16} - \Gamma/\sqrt{2}$ . As can be seen from Fig. 2, the PTMC result agrees well with the exact one. All the transitions are of first order because of the kinks in the energy curve.

*Intermediate gapless QSL phase.* – It has been firmly established that the quantum ground state of Eq. (1) is a zigzag order[61] or stripy order[62] in the limiting cases where  $\vartheta/\pi = 0$  or 1, respectively. Although both phases break translational symmetry, they possess different symmetries in that the former owns  $C_2$  rotational symmetry while the latter has mirror symmetry. According to Landau’s theory, we would expect that the transition between the zigzag phase and the stripy phase is of first order, if it occurs. However, due to the interplay between Heisenberg and  $\Gamma$  interactions, the direct transition is forbidden, leading to an intermediate phase whose ground-state energy per site  $e_g = E_g/N$  has an inconspicuous change versus  $\vartheta$  (see Fig. 3(a)). Surprisingly, as shown in the inset, the energy  $e_g$  at  $\vartheta/\pi = 0.5$  exhibits a nonmonotonic fall with the increasing of circumference  $n$  because of the overwhelming subnormal energy for  $n = 6$ . Such a nonmonotonic behavior is also discussed in a recent work[53]. We mention here that this phenomenon is observed only in the quantum case and does not exist in its classical analogy[60]. By the linear extrapolation of energy  $e_g$  with the two largest sizes, we find that the energy at  $\vartheta/\pi = 0.5$  is approximately  $e_g = -0.3542(3)$ , which is only slightly lower than that of  $n = 6$ . Therefore, were the counterintuitive phenomenon not seriously considered, a misleading conclusion would be arrived at when the system size is not large enough. The energy  $e_g$  has two forceful downwarping, leading to two well-marked kinks. The kinks in the energy curve are signals of first-order phase transitions. In Fig. 3(b) we show the evolution of two lowest excitation gaps,  $\Delta_{1,2} = E_{1,2} - E_g$ , the energy difference between the first/second excited states  $E_{1,2}$  and the ground state  $E_g$ . Due to the two nonequivalent sites in one unit cell, both the zigzag and stripy phases have two-fold degeneracy. Therefore,  $\Delta_1$  should vanish while  $\Delta_2$  is finite. When approaching the two separate transition points,  $\Delta_2$  decreases, and finally vanishes in the intermediate phase. Besides, the von Neumann entropy in this phase is much larger than that in the gapped phases, and it increases with the total size[60]. In particular, we do not detect the other intermediate phase as compared to the classical situation in our precision and resolution. All together, we could safely arrive at the conclusion that there is a gapless intermediate phase when  $\vartheta_{t,l}/\pi \leq \vartheta/\pi \leq \vartheta_{t,r}/\pi$  with  $\vartheta_{t,l}/\pi \simeq 0.50$  and  $\vartheta_{t,r}/\pi = 0.66(1)$ . Interestingly, both

$\vartheta_{t,l}$  and  $\vartheta_{t,r}$  agree with their classical counterparts.

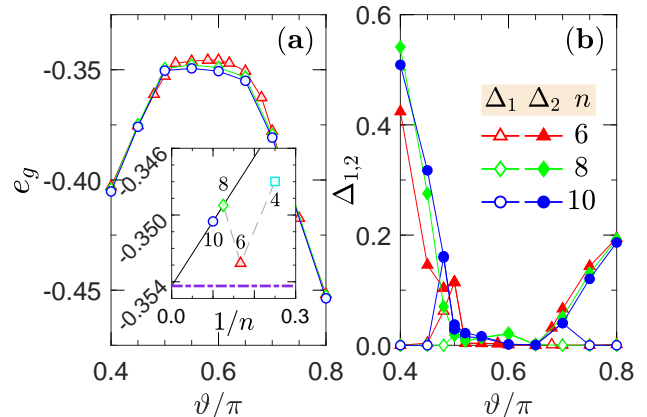


FIG. 3: (a) The ground-state energy per site  $e_g$  for  $\vartheta/\pi$  ranging from 0.4 to 0.8. The circumferences  $n$  of the clusters are 6 (red triangle), 8 (green diamond), and 10 (blue circle). Inset: Linear extrapolations of  $e_g$  at  $\vartheta/\pi = 0.5$  with  $n = 8$  and 10. (b) The two lowest excitation gaps  $\Delta_1$  (open symbols) and  $\Delta_2$  (filled symbols).

Now we turn to measure the magnetic order by calculating the static magnetic structure factors (SMSF),  $\mathcal{S}_N(\mathbf{Q}) = \sum_{\alpha\beta} \delta_{\alpha\beta} \mathcal{S}_N^{\alpha\beta}(\mathbf{Q})$ , where  $\mathcal{S}_N^{\alpha\beta}(\mathbf{Q}) = \frac{1}{N} \sum_{ij} \langle S_i^\alpha S_j^\beta \rangle e^{i\mathbf{Q} \cdot (\mathbf{R}_i - \mathbf{R}_j)}$ . The order parameter is thus characterized by  $M_N(\mathbf{Q}) = \sqrt{\mathcal{S}_N(\mathbf{Q})/N}$  with  $\mathbf{Q}$  being the corresponding ordering wavevector. As can be seen from Fig. 4(a), when varying  $\vartheta/\pi$  from 0 to 1, we find that the order parameters in both zigzag and stripy orders show nonmonotonic behaviors and they exhibit maxima at  $\vartheta/\pi \approx 0.25$  and  $0.75$ , respectively. This suggests that the magnetic orders are most stable when  $\Gamma$  term is approximately of equal strength to the Heisenberg interaction. Away from those points, the quantum fluctuations are enhanced and novel phase may possibly appear. This is indeed observed in  $M_N(\mathbf{Q})$  as we show in Fig. 4(a). In the intermediate region, the magnetic order is dramatically suppressed. It decreases with the increasing of circumference  $n$ . After a careful inspection of the finite-size effect (see Fig. 4(b) and Fig. 4(c)), it approaches zero in the thermodynamic limit (TDL), indicating that the intermediate phase is a magnetically disordered phase. Moreover, we check the magnetic order at  $\vartheta/\pi = 0.5$  carefully (see Fig. 4(b)) and a linear extrapolation of the raw data gives us  $M \approx -0.0065$  at infinite size. However, such magnetic order could be corrected to  $M \simeq 0.0000(2)$  if we ignore the data at  $n = 6$ . The energy  $e_g$  at this cluster is close to that in the TDL (see Fig. 3) and there is no wonder that it has a smaller magnetic order and thus deviates slightly from the scaling line. Again, our results do not support two intermediate phases discussed in the classical phase diagram. We refer to the argument for a similar anisotropic model on triangular lattice which is proposed for the QSL candidate  $\text{YbMgGaO}_4$ [3]. Whereas

a so-called multi- $\mathbf{Q}$  phase exists between two magnetically ordered phases[63] in the classical phase diagram, extensive DMRG calculations do not detect its trail in the quantum model, but instead suggest a direct first-order phase transition[64, 65].

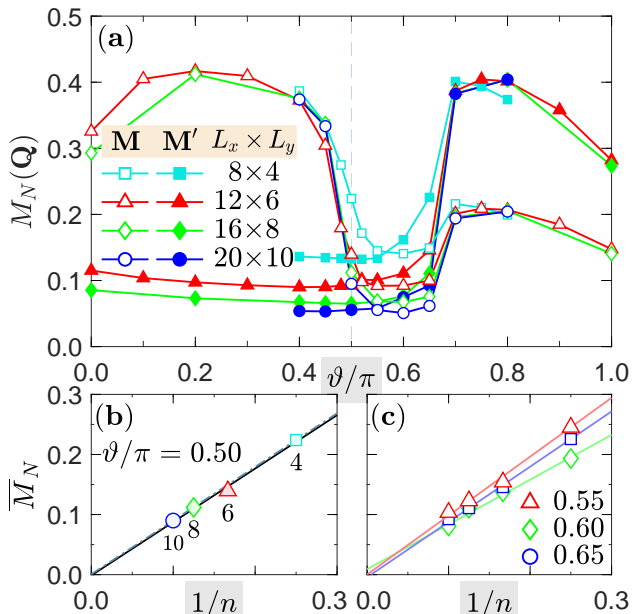


FIG. 4: (a) Order parameters  $M_N(\mathbf{Q})$  for the zigzag order (open symbols) and stripy order (filled symbols) with  $\mathbf{Q} = \mathbf{M}$  and  $\mathbf{M}'$ , respectively. The circumferences  $n$  of the clusters are 4 (cyan squares), 6 (red triangles), 8 (green diamonds), and 10 (blue circles). (b) Linear extrapolations of the maximal order parameter  $\bar{M}_N$  at  $\vartheta/\pi = 0.5$  with (solid) and without (dotted) the data for  $n = 6$ . (c) Linear extrapolations of the magnetic order at  $\vartheta/\pi = 0.55$  (red triangle),  $0.60$  (green diamond), and  $0.65$  (blue circle).

The quantum phase diagram of the bond-modulated spin-1/2  $J$ - $\Gamma$  model is shown in Fig. 5. There is a zigzag phase for  $\vartheta < \vartheta_{t,l}$ , a stripy phase for  $\vartheta > \vartheta_{t,r}$ , and a gapless QSL phase sandwiched between the two with  $\vartheta_{t,l}/\pi \simeq 0.50$  and  $\vartheta_{t,r}/\pi = 0.66(1)$ . We emphasize here that a gapless QSL phase is found in a quite large region between  $\vartheta_{t,l}$  and  $\vartheta_{t,r}$  with  $\vartheta_{t,r} - \vartheta_{t,l} \approx \pi/6$ . The transitions between the QSL phase and the zigzag/stripy phases are both of first order, which can be inferred either from the kinks in the energy curve (see Fig. 3(a)) or from the jumps in the magnetic order parameters (see Fig. 4(a)). The selected contour plots of the SMSF for the three phases are shown in Fig. 5(a)-(c). While the zigzag and stripy phases peak at  $\mathbf{M}$  and  $\mathbf{M}'$  points, respectively, the magnetic order at  $\vartheta/\pi = 0.50$  is dramatically suppressed. Interestingly, a subleading peak locating at  $\mathbf{X}$  point in the Brillouin zone appears. This peak could be enhanced by negative third-NN interaction[60].

*Pinning the magnetic orders.* – We resort to a complementary technique proposed recently by Zhu *et. al.*[58] to provide further evidence for the QSL phase in Eq. (1).

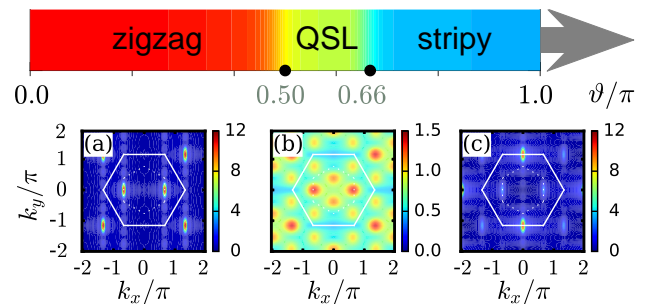


FIG. 5: Quantum phase diagram of the bond-modulated spin-1/2  $J$ - $\Gamma$  model on a honeycomb lattice. The shade of color is a reminiscence of the corresponding magnetic order. Typical contour plots of the overall SMSF for (a) zigzag phase ( $\vartheta/\pi = 0.25$ ), (b) QSL phase ( $\vartheta/\pi = 0.50$ ), and (c) stripy phase ( $\vartheta/\pi = 0.75$ ) are shown for XC clusters of  $12 \times 6$ .

Unlike in the conventional CBC where all the parameters are fixed, the spirit of the method is that the control parameter  $\vartheta$  is varied in  $x$  direction of the cylinder, and thus local spin patterns provide a reliable visual display of existing phases[58, 65]. This method is born to detect the intermediate disordered phase sandwiched between two magnetically ordered phases and has been successfully applied to several different models[58, 65, 66]. Generally, the length of the cylinder should not be too small so as to release the magnetic order in the middle region. we adopt a fixed aspect ratio  $L_x/L_y = 6$ , which could be explained as a triplet assembly of the conventional geometry. The range of the varied parameter is also of vital importance to minimize the ineluctable proximity effect, and the best choice for us is  $\vartheta_{\min}/\pi = 49/120$  and  $\vartheta_{\max}/\pi = 91/120$ . Within this interval, we take a  $0.01\pi$  increment for two successive columns. The pinning fields which are consistent with the zigzag and stripy orders are applied to the spins at the leftmost and rightmost columns, respectively[60].

We present the visual display of the spin configuration on the long cylinder of  $L_y = 6$  in Fig. 6. the spin patterns evolve smoothly from a zigzag order to a stripy order. Remarkably, a plausible disordered phase with amorphous orientation of spins appears in the middle. Fig. 7 shows the local ordered moment  $\langle S_{\text{tot}} \rangle$ . Because of the pinning fields utilized, the moments shows an artificial upwarping at the boundaries. The  $x$  and  $y$  components have a almost equal magnitude all the way while the  $z$  component in the stripy phase is disordered. The total order in the middle is rather weak and we use a threshold value of  $\langle S_{\text{tot}} \rangle \approx 0.10$  as the upper limit of the disordered phase for the current system size[58, 65]. Interestingly, the rough phase boundaries of the disordered phase ( $0.50 \leq \vartheta/\pi \lesssim 0.65$ ) are fairly consistent with those obtained in previous DMRG calculations. It should be noted that whereas the pinning order at  $\vartheta/\pi = 0.50$  is not small enough, we would expect a rapid decay if

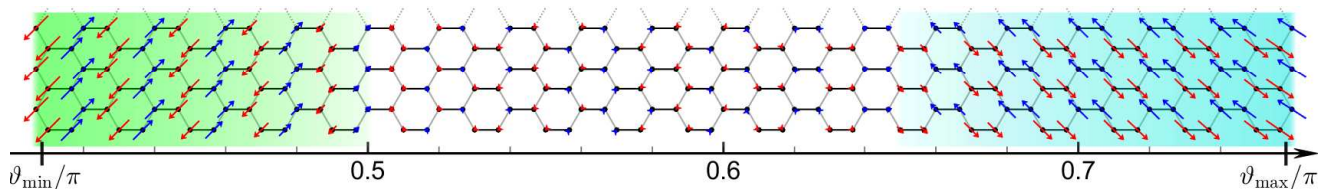


FIG. 6: For a long XC cylinder of  $36 \times 6$ , we vary  $\vartheta/\pi$  with position, from  $\vartheta_{\min}/\pi = 49/120$  on the left edge to  $\vartheta_{\max}/\pi = 91/120$  on the right edge. We also apply pinning magnetic fields along all the three spin directions on the left (right) edge to favor the classical zigzag (stripy) order. The length of the arrow represents local measurement of  $\langle S_{\text{tot}} \rangle = \sqrt{\langle S_x \rangle^2 + \langle S_y \rangle^2 + \langle S_z \rangle^2}$ , and an intermediate disordered phase without the shadow is revealed to sandwich between the two.

we can access larger clusters. It is in this sense that we confirm the robustness of an intermediate disordered phase in the quantum phase diagram of the Hamiltonian Eq. (1).

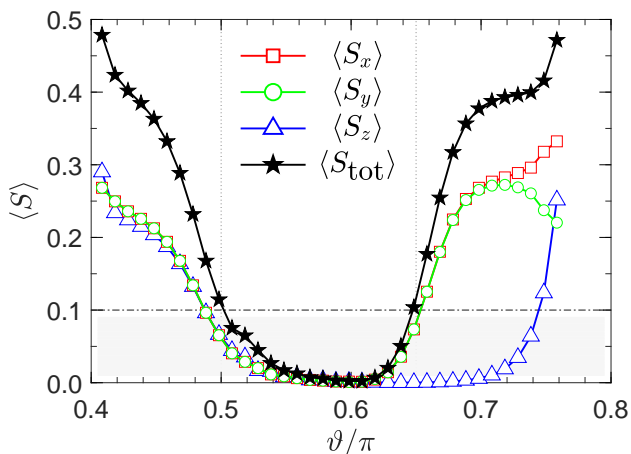


FIG. 7: DMRG results for local moment  $\langle S_{\text{tot}} \rangle$  vs  $\vartheta$  for XC cluster of  $36 \times 6$ . The dotted vertical lines denote the possible phase boundaries.

*Summary.* – To conclude, we have studied the phase diagram of a bond-modulated spin-1/2  $J$ - $\Gamma$  model on a honeycomb lattice. We find that, apart from zigzag and stripy magnetically ordered phases, there are still two intermediate phases but with dramatically different interval ranges in the classical phase diagram. In the quantum case, a gapless QSL phase emerges between the zigzag phase and the stripy phase. It is separated from its two neighbors by first-order phase transitions, and the ground state of the HCTA happens to locate at its leftmost side. Our results thus clarify the momentous controversy on the HCTA model and provide a significant guidance to further theoretical studies on the generic anisotropic model on a honeycomb lattice as well as to unveil the microscopic Hamiltonian that could describe the Kitaev material  $\alpha$ - $\text{RuCl}_3$ .

*Acknowledgements* – We thank S. Hu for fruitful discussions during the collaboration on related topics. We also thank M. Gohlke, Y.-Z. Huang, H.-Y. Kee, T. Li, H.-J. Liao, K. Liu, Z.-X. Liu, B. Xi, and W. Yu for helpful dis-

cussions. J.Z. was supported by the the National Natural Science Foundation of China (Grant No. 11874188) and the Fundamental Research Funds for the Central Universities. X.W. was supported by the National Program on Key Research Project (Grant No. 2016YFA0300501) and by the National Natural Science Foundation of China (Grants No. 11574200 and No. 11974244).

\* zhaojz@lzu.edu.cn

† xiaoqunwang@sjtu.edu.cn

- [1] L. Balents, Nature (London) **464**, 199 (2010).
- [2] T.-H. Han, J. S. Helton, S. Chu, D. G. Nocera, J. A. Rodriguez-Rivera, C. Broholm, and Y. S. Lee, Nature (London) **492**, 406 (2012).
- [3] Y. Li, G. Chen, W. Tong, L. Pi, J. Liu, Z. Yang, X. Wang, and Q. Zhang, Phys. Rev. Lett. **115**, 167203 (2015).
- [4] H. J. Liao, Z. Y. Xie, J. Chen, Z. Y. Liu, H. D. Xie, R. Z. Huang, B. Normand, and T. Xiang, Phys. Rev. Lett. **118**, 137202 (2017).
- [5] K. W. Plumb, J. P. Clancy, L. J. Sandilands, V. V. Shankar, Y. F. Hu, K. S. Burch, H.-Y. Kee, and Y.-J. Kim, Phys. Rev. B **90**, 041112(R) (2014).
- [6] A. Banerjee, C. A. Bridges, J.-Q. Yan, A. A. Aczel, L. Li, M. B. Stone, G. E. Granroth, M. D. Lumsden, Y. Yiu, J. Knolle, S. Bhattacharjee, D. L. Kovrizhin, R. Moessner, D. A. Tennant, D. G. Mandrus, and S. E. Nagler, Nat. Mater. **15**, 733 (2016).
- [7] A. Banerjee, J. Yan, J. Knolle, C. A. Bridges, M. B. Stone, M. D. Lumsden, D. G. Mandrus, D. A. Tennant, R. Moessner, and S. E. Nagler, Science **356**, 1055 (2017).
- [8] J. G. Rau, E. K.-H. Lee, and H.-Y. Kee, Annu. Rev. Condens. Matter Phys. **7**, 195 (2016).
- [9] G. Jackeli and G. Khaliullin, Phys. Rev. Lett. **102**, 017205 (2009).
- [10] Z. Nussinov and J. van den Brink, Rev. Mod. Phys. **97**, 1 (2015).
- [11] A. Kitaev, Ann. Phys. **321**, 2 (2006).
- [12] F. Ye, S. X. Chi, H. B. Cao, B. C. Chakoumakos, J. A. Fernandez-Baca, R. Custelcean, T. F. Qi, O. B. Korneta, and G. Cao, Phys. Rev. B **85**, 180403 (2012).
- [13] S. K. Choi, R. Coldea, A. N. Kolmogorov, T. Lancaster, I. I. Mazin, S. J. Blundell, P. G. Radaelli, Y. Singh, P. Gegenwart, K. R. Choi, S.-W. Cheong, P. J. Baker, C. Stock, and J. Taylor, Phys. Rev. Lett. **108**, 127204 (2012).
- [14] S. H. Chun, J.-W. Kim, J. Kim, H. Zheng, C. C.

- Stoumpos, C. D. Malliakas, J. F. Mitchell, K. Mehlawat, Y. Singh, Y. Choi, T. Gog, A. Al-Zein, M. M. Sala, M. Krisch, J. Chaloupka, G. Jackeli, G. Khaliullin, and B. J. Kim, *Nat. Phys.* **11**, 462 (2015).
- [15] J. A. Sears, M. Songvilay, K. W. Plumb, J. P. Clancy, Y. Qiu, Y. Zhao, D. Parshall, and Y.-J. Kim, *Phys. Rev. B* **91**, 144420 (2015).
- [16] I. A. Leahy, C. A. Pocs, P. E. Siegfried, D. Graf, S.-H. Do, K.-Y. Choi, B. Normand, and M. Lee, *Phys. Rev. Lett.* **118**, 187203 (2017).
- [17] J. A. Sears, Y. Zhao, Z. Xu, J. W. Lynn, and Y.-J. Kim, *Phys. Rev. B* **95**, 180411(R) (2017).
- [18] S.-H. Baek, S.-H. Do, K.-Y. Choi, Y. S. Kwon, A. U. B. Wolter, S. Nishimoto, J. van den Brink, and B. Büchner, *Phys. Rev. Lett.* **119**, 037201 (2017).
- [19] A. U. B. Wolter, L. T. Corredor, L. Janssen, K. Nenkov, S. Schönecker, S.-H. Do, K.-Y. Choi, R. Albrecht, J. Hunger, T. Doert, M. Vojta, and B. Büchner, *Phys. Rev. B* **96**, 041405(R) (2017).
- [20] Z. Wang, S. Reschke, D. Hüvonen, S.-H. Do, K.-Y. Choi, M. Gensch, U. Nagel, T. Room, and A. Loidl, *Phys. Rev. Lett.* **119**, 227202 (2017).
- [21] J. Zheng, K. Ran, T. Li, J. Wang, P. Wang, B. Liu, Z.-X. Liu, B. Normand, J. Wen, and W. Yu, *Phys. Rev. Lett.* **119**, 227208 (2017).
- [22] L. J. Sandilands, Y. Tian, K. W. Plumb, Y.-J. Kim, and K. S. Burch, *Phys. Rev. Lett.* **114**, 147201 (2015).
- [23] G. Li, X. Chen, Y. Gan, F. Li, M. Yan, S. Pei, Y. Zhang, L. Wang, H. Su, J. Dai, Y. Chen, Y. Shi, X. Wang, L. Zhang, S. Wang, D. Yu, F. Ye, J.-W. Mei, and M. Huang, *Phys. Rev. Materials* **3**, 023601 (2019).
- [24] S.-H. Do, S.-Y. Park, J. Yoshitake, J. Nasu, Y. Motome, Y. S. Kwon, D. T. Adroja, D. J. Voneshen, K. Kim, T.-H. Jang, J.-H. Park, K.-Y. Choi, and S. Ji, *Nat. Phys.* **13**, 1079 (2017).
- [25] K. Ran, J. Wang, W. Wang, Z.-Y. Dong, X. Ren, S. Bao, S. Li, Z. Ma, Y. Gan, Y. Zhang, J. T. Park, G. Deng, S. Danilkin, S.-L. Yu, J.-X. Li, and J. Wen, *Phys. Rev. Lett.* **118**, 107203 (2017).
- [26] S. M. Winter, K. Riedl, P. A. Maksimov, A. L. Chernyshev, A. Honecker, and R. Valenti, *Nat. Commun.* **8**, 1152 (2018).
- [27] H.-C. Jiang, Z.-C. Gu, X.-L. Qi, and S. Trebst, *Phys. Rev. B* **83**, 245104 (2011).
- [28] L. Janssen, E. C. Andrade, and M. Vojta, *Phys. Rev. Lett.* **117**, 277202 (2016).
- [29] G.-W. Chern, Y. Sizyuk, C. Price, and N. B. Perkins, *Phys. Rev. B* **95**, 144427 (2017).
- [30] Z. Zhu, I. Kimchi, D. N. Sheng, and L. Fu, *Phys. Rev. B* **97**, 241110(R) (2018).
- [31] M. Gohlke, R. Moessner, and F. Pollmann, *Phys. Rev. B* **98**, 014418 (2018).
- [32] S. Liang, M.-H. Jiang, W. Chen, J.-X. Li, and Q.-H. Wang, *Phys. Rev. B* **98**, 054433 (2018).
- [33] J. Nasu, Y. Kato, Y. Kamiya, and Y. Motome, *Phys. Rev. B* **98**, 060416(R) (2018).
- [34] H.-C. Jiang, C.-Y. Wang, B. Huang, and Y.-M. Lu, [arXiv:1809.08247](https://arxiv.org/abs/1809.08247) (2018).
- [35] C. Hickey and S. Trebst, *Nat. Commun.* **10**, 530 (2019).
- [36] M. Hermanns, I. Kimchi, J. Knolle, *Annu. Rev. Condens. Matter Phys.* **9**, 17 (2018).
- [37] Y. D. Li, X. Yang, Y. Zhou, G. Chen, *Phys. Rev. B* **99**, 205119 (2019).
- [38] L. Janssen, E. C. Andrade, and M. Vojta, *Phys. Rev. B* **96**, 064430 (2017).
- [39] J. G. Rau, E. K.-H. Lee, and H.-Y. Kee, *Phys. Rev. Lett.* **112**, 077204 (2014).
- [40] R. Yadav, N. A. Bogdanov, V. M. Katukuri, S. Nishimoto, J. van den Brink, and L. Hozoi, *Sci. Rep.* **6**, 37925 (2016).
- [41] Z.-X. Liu and B. Normand, *Phys. Rev. Lett.* **120**, 187201 (2018).
- [42] L. Zou and Y.-C. He, [arXiv:1809.09091](https://arxiv.org/abs/1809.09091) (2018).
- [43] G. Wachtel and D. Orgad, *Phys. Rev. B* **99**, 115104 (2019).
- [44] J. S. Gordon, A. Catuneanu, E. S. Sørensen, and H.-Y. Kee, *Nat. Commun.* **10**, 2470 (2019).
- [45] D. Takikawa and S. Fujimoto, *Phys. Rev. B* **99**, 224409 (2019).
- [46] P. Lampen-Kelley, S. Rachel, J. Reuther, J.-Q. Yan, A. Banerjee, C. A. Bridges, H. B. Cao, S. E. Nagler, D. Mandrus, *Phys. Rev. B* **98**, 100403(R) (2018).
- [47] J. Nasu, M. Udagawa, and Y. Motome, *Phys. Rev. B* **92**, 115122 (2015).
- [48] I. Rousochatzakis and N. B. Perkins, *Phys. Rev. Lett.* **118**, 147204 (2017).
- [49] A. M. Samarakoon, G. Wachtel, Y. Yamaji, D. A. Tennant, C. D. Batista, and Y. B. Kim, *Phys. Rev. B* **98**, 045121 (2018).
- [50] A. Catuneanu, Y. Yamaji, G. Wachtel, Y.-B. Kim, and H.-Y. Kee, *npj Quantum Materials* **3**, 23 (2018).
- [51] M. Gohlke, G. Wachtel, Y. Yamaji, F. Pollmann, and Y. B. Kim, *Phys. Rev. B* **97**, 075126 (2018).
- [52] P. Saha, Z. Fan, D. Zhang, and G.-W. Chern, *Phys. Rev. Lett.* **122**, 257204 (2019).
- [53] J. Wang, B. Normand, and Z.-X. Liu, [arXiv:1903.10026](https://arxiv.org/abs/1903.10026) (2019).
- [54] S. R. White, *Phys. Rev. Lett.* **69**, 2863 (1992).
- [55] E. M. Stoudenmire and S. R. White, *Annu. Rev. Condens. Matter Phys.* **3**, 111 (2012).
- [56] N. Metropolis, A. W. Rosenbluth, M. N. Rosenbluth, A. H. Teller, and E. Teller, *J. Chem. Phys.* **21**, 1087 (1953).
- [57] K. Hukushima and K. Nemoto, *J. Phys. Soc. Jpn.* **65**, 1604 (1996).
- [58] Z. Zhu, D. A. Huse, and S. R. White, *Phys. Rev. Lett.* **111**, 257201 (2013).
- [59] S.-S. Gong, D. N. Sheng, O. I. Motrunich, and M. P. A. Fisher, *Phys. Rev. B* **88**, 165138 (2013).
- [60] See Supplemental Material at [url] for configurations of classical phases, entropy of the quantum model, role of third-NN interaction, and ideas on the long cylinder.
- [61] Y.-Z. Huang, B. Xi, X. Chen, W. Li, Z.-C. Wang, and G. Su, *Phys. Rev. E* **93**, 062110 (2016).
- [62] Y.-Z. Huang and G. Su, *Phys. Rev. E* **95**, 052147 (2017).
- [63] C. Liu, R. Yu, and X. Wang, *Phys. Rev. B* **94**, 174424 (2016).
- [64] Q. Luo, S. Hu, B. Xi, J. Zhao, and X. Wang, *Phys. Rev. B* **95**, 165110 (2017).
- [65] Z. Zhu, P. A. Maksimov, S. R. White, and A. L. Chernyshev, *Phys. Rev. Lett.* **119**, 157201 (2017).
- [66] Z. Zhu and S. R. White, *Phys. Rev. B* **92**, 041105(R) (2015).

# Supplemental Material for “Gapless spin liquid state of the spin- $\frac{1}{2}$ honeycomb antiferromagnetic $\Gamma$ model”

Qiang Luo<sup>1</sup>, Jize Zhao<sup>2</sup>, and Xiaoqun Wang<sup>3,4</sup>

<sup>1</sup>Department of Physics, Renmin University of China, Beijing 100872, China

<sup>2</sup>School of Physical Science and Technology & Key Laboratory for Magnetism and Magnetic Materials of the MoE, Lanzhou University, Lanzhou 730000, China

<sup>3</sup>Key Laboratory of Artificial Structures and Quantum Control (Ministry of Education), School of Physics and Astronomy, Tsung-Dao Lee Institute, Shanghai Jiao Tong University, Shanghai 200240, China

<sup>4</sup>Beijing Computational Science Research Center, Beijing 100084, China

## CONFIGURATIONS OF CLASSICAL PHASES

### Ground state of the classical $\Gamma$ model

The ground state of the classical  $\Gamma$  model is known to be the classical spin liquid[1]. For the model (1) considered in the main text, it locates at the transition point between the zigzag phase and the mixed phase. Because of the two-sublattice (say  $\{S_a\}$  and  $\{S_b\}$ ) nature of the adjacent phases, the classical spins that contribute to the ground-state manifolds should only satisfy the condition that half of them are parallel to  $S_a$  while the rest are parallel to  $S_b$ , regardless of the positions. Therefore, the degeneracy of the ground state is of the order  $\mathcal{O}(2^N/\sqrt{N})$  where  $N$  is the total number of spins. The typical static magnetic structure factor (SMSF) is shown in Fig. SM-1, which is featureless as expected.

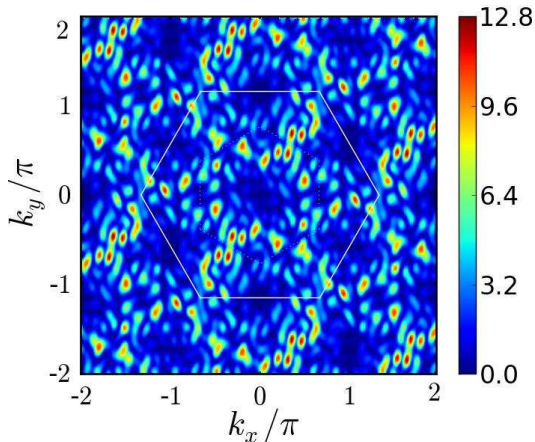


FIG. SM-1: Typical SMSF of the classical  $\Gamma$  model with the system size  $L_x \times L_y = 16 \times 16$ .

As shown in the main text, the ground-state energy per site (*i.e.*, in unit of  $NS^2$ )  $e_g$  is exactly  $-1$ . To study how does the energy at finite size evolve toward infinite size, we calculate the classical energy at different sizes. Here, both cylindrical boundary condition (CBC) and toroidal boundary condition (TBC) are utilized but with different aspect ratio  $L_x/L_y$ , which is 2 for the former and

1 for the latter. It could be observed in Fig. SM-2 that the energy  $e_g$  does not show any finite-size effect under TBC, while it obeys a linear scaling law under CBC. In the thermodynamic limit, it is  $-1$  for both cases.

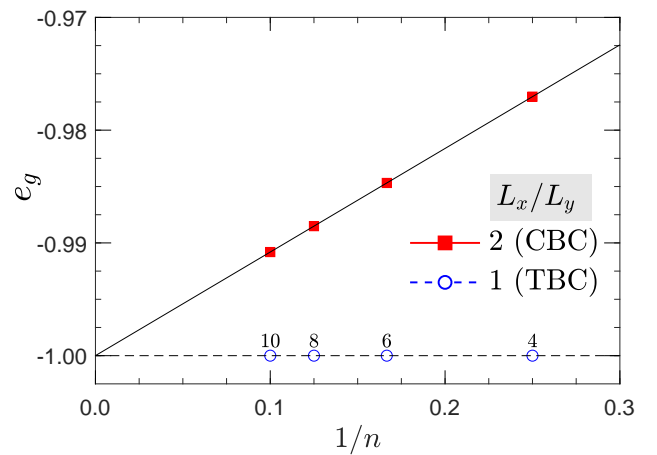


FIG. SM-2: Classical ground-state energy  $e_g$  of  $\Gamma$  model under CBC with  $L_x/L_y = 2$  (red square) and TBC with  $L_x/L_y = 1$  (blue circle).

### The zigzag and stripy phases

In this part we will go into the zigzag and stripy phases shown in Fig. 1 of the main text. The zigzag order can be described as ferromagnetic zigzag chains coupled antiferromagnetically. The stripe order, on the contrary, is formed by antiferromagnetic zigzag chains with ferromagnetic coupling. Both phases could be divided into two sublattices with opposite spins. The classical spin, which is an  $O(3)$  vector, can be written as

$$\mathbf{S}_i = S (\sin \theta_i \cos \phi_i, \sin \theta_i \sin \phi_i, \cos \theta_i), \quad (\text{SM-1})$$

where  $\theta_i \in [0, \pi)$  and  $\phi_i \in [0, 2\pi)$  are respectively the polar and azimuthal angles at site  $i$ . Suppose that one sublattice has the angles  $(\theta, \phi)$ , then the other sublattice has the angles  $(\pi - \theta, \pi + \phi)$ . The three bonds (*i.e.*,  $\mathbf{X}$ ,  $\mathbf{Y}$ , and  $\mathbf{Z}$  bonds) have different contributions to the total

energy and should be considered separately. After adding up all the terms, we find that the energies per site in the two phases are

$$e_g^{\text{zigzag}} = -\frac{1}{2}(3J + \mathcal{F}_{\max}(\theta, \phi)\Gamma) \quad (\text{SM-2})$$

and

$$e_g^{\text{stripy}} = \frac{1}{2}(3J + \mathcal{F}_{\min}(\theta, \phi)\Gamma) \quad (\text{SM-3})$$

where an auxiliary function  $\mathcal{F}(\theta, \phi)$  is introduced naturally. It is worth mentioning that whereas  $\Gamma$  is always nonnegative, the Heisenberg interaction  $J$  is positive (negative) in the zigzag (stripy) phase. The explicit form of the function is

$$\mathcal{F}(\theta, \phi) = \sin^2 \theta \sin 2\phi - \sin 2\theta(\sin \phi + \cos \phi). \quad (\text{SM-4})$$

Its maximum is 2 with  $(\theta, \phi) = (\pi - \text{atan}(\sqrt{2}), \pi/4)$  or  $(\theta, \phi) = (\text{atan}(\sqrt{2}), 5\pi/4)$  and its minimum is  $-1$ , see Fig. SM-3. All the critical points are given by the following identify

$$\tan 2\theta = \frac{1}{\sin \phi} + \frac{1}{\cos \phi}. \quad (\text{SM-5})$$

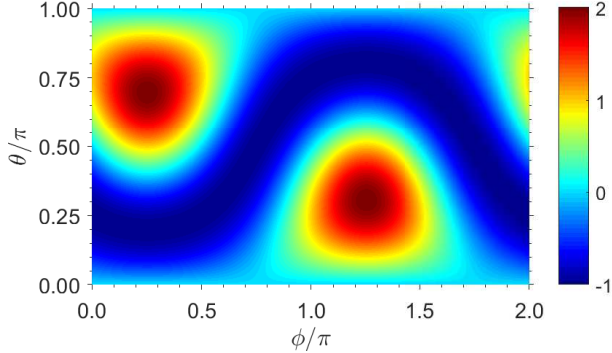


FIG. SM-3: Illustration of function  $\mathcal{F}(\theta, \phi)$  (see Eq. (SM-4)) in the whole parameter region.

The classical energy of the zigzag phase is  $e_g^{\text{zigzag}} = -(2\Gamma + 3J)/2$ , and the angles of the spins are either  $(\theta, \phi) = (\pi - \text{atan}(\sqrt{2}), \pi/4)$  or  $(\theta, \phi) = (\text{atan}(\sqrt{2}), 5\pi/4)$ . Interestingly, the three components of the spin vector have an equal strength of  $\sqrt{3}/3$ . The energy of the stripy phase is  $e_g^{\text{stripy}} = -(\Gamma - 3J)/2$ , and the angles satisfy the restriction Eq. (SM-5). Since there are infinite solutions to Eq. (SM-5) which span in a certain locus as shown in Fig. SM-3, we conclude that there is an emergent continuous symmetry in the classical stripy phase.

#### The mixed AFM–twining zigzag phase

Due to the bond-modulated  $\eta_{ij}(\pm 1)$  term, the underlying honeycomb lattice does not possess  $C_6$  rotational

symmetry. Therefore, the intuition that the zigzag order has three degenerate configurations is not correct here. We find that the other two twining zigzag orders (see Fig. SM-4(b) and (c)) have higher energy than the zigzag order (see Fig. 1(c) of the main text) when  $\vartheta/\pi \in [0, 1/2)$ . When  $\vartheta/\pi$  is slightly larger than  $1/2$ , the twining zigzag orders overcome the latter and become the ground state. Interestingly, the AFM order (see Fig. SM-4(a)) has the same energy and contributes to the degenerate manifolds. Moreover, due to the two nonequivalent sites per unit cell, each configuration is two-fold degenerate. Consequently, we conclude that the mixed phase has six-fold degenerate ground states.

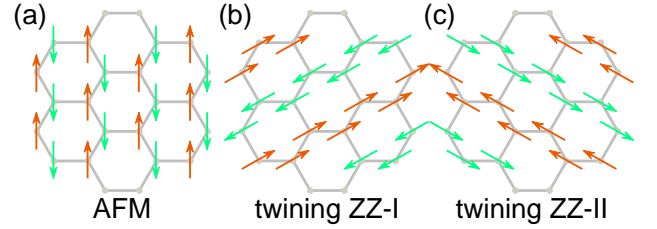


FIG. SM-4: The degenerate ground states of the mixed phase, which includes (a) AFM order and (b)/(c) two kinds of twining zigzag orders.

The energy of the mixed phase is given by

$$e_g^{\text{mixed}} = -\frac{1}{2}(-J + \mathcal{F}_{\max}(\theta, \phi + \pi)\Gamma). \quad (\text{SM-6})$$

Since the translation of  $\phi$  by  $\pi$  does not change the magnitude of the function  $\mathcal{F}(\theta, \phi)$ , we then obtain  $e_g^{\text{mixed}} = -(2\Gamma - J)/2$  with  $(\theta, \phi) = (\text{atan}(\sqrt{2}), \pi/4)$  or  $(\theta, \phi) = (\pi - \text{atan}(\sqrt{2}), 5\pi/4)$ .

#### The noncoplanar phase

In addition to the zigzag phase, the stripy phase, and the mixed phase discussed above, there is a noncoplanar (NCP) phase consisting of two kinds of spins (or four if we consider that two of them are anti-parallel to their partners) which are neither (anti-)parallel nor perpendicular in the classical phase diagram. Suppose that the angles of one kind of the spins are  $(\theta, \phi)$ , then they are  $(\theta + \pi/2, \phi + \pi)$  for the other. Namely,

$$\begin{cases} \mathbf{S}_a = S(\sin \theta \cos \phi, \sin \theta \sin \phi, \cos \theta) \\ \mathbf{S}_b = -S(\cos \theta \cos \phi, \cos \theta \sin \phi, \sin \theta) \end{cases}. \quad (\text{SM-7})$$

One of the configurations of the spins is shown in Fig. SM-5(a). The optimal angles could be obtained by minimizing the classical energy

$$e_g^{\text{NCP}} = J \sin 2\theta + \frac{\Gamma}{4}[\cos 2\theta \sin 2\phi - 2(\sin \phi + \cos \phi)]. \quad (\text{SM-8})$$

For example, if  $\theta = 3\pi/4 - \psi_0/2$  and  $\phi = \pi/4$  where  $\psi_0 = \text{atan}(\frac{\Gamma}{4J})$ , we have the classical energy

$$e_g^{\text{NCP}} = -\sqrt{J^2 + \frac{\Gamma^2}{16}} - \frac{\Gamma}{\sqrt{2}}. \quad (\text{SM-9})$$

We also note that the angles between the two kinds of spins are  $-\psi_0$  or its supplementary angle  $\pi + \psi_0$ . Since  $\psi_0$  is  $\vartheta$ -dependent, the polar angle  $\theta$  also varies with  $\vartheta$ .

The fascinating character of the NCP phase is that it may also possess other ground states with larger unit cell. For example, we find such a ground state whose unit cell has 64 lattice sites, see Fig. SM-5(b).

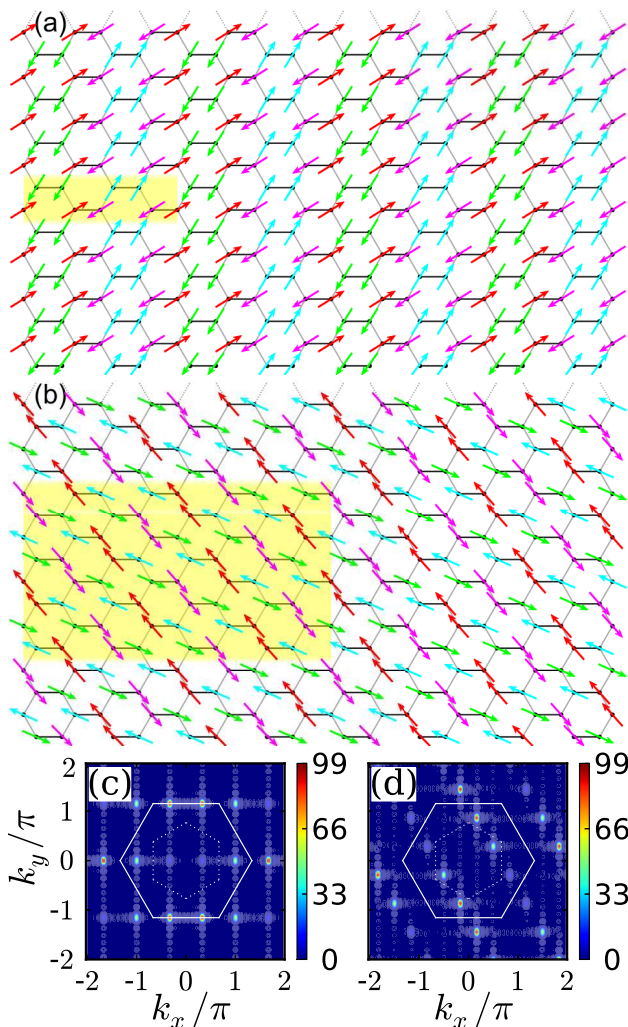


FIG. SM-5: Configurations of the noncoplanar phase in the real space. The size of the unit cell marked by the yellow shadow is (a)  $4 \times 2$  and (b)  $8 \times 8$ . Their SMSFs in the momentum space are shown in (c) and (d), respectively.

## ENTROPY OF THE QUANTUM MODEL

The von Neumann entropy (vNE)  $\mathcal{S}$ , which is frequently used to characterize different phases, is readily available because the lattice is intrinsically divided into two parts, say  $s$  and  $e$ , in our DMRG simulations. Therefore,  $\mathcal{S} = -\text{Tr}(\rho_s \ln \rho_s)$  where the reduced density matrix  $\rho_s = \text{Tr}_e |\psi\rangle\langle\psi|$  is obtained by tracing out the degrees of freedom of  $e$ . We present our results in Fig. SM-6 where three XC clusters of  $12 \times 6$ ,  $16 \times 8$ , and  $20 \times 10$  are included. It shows that the vNE in the gapped zigzag and stripy phases are lower than that in the intermediate phase. Besides, with the increasing of the total sites  $S$  in the intermediate phase increases. This agrees with our conclusion that the intermediate phase is gapless.

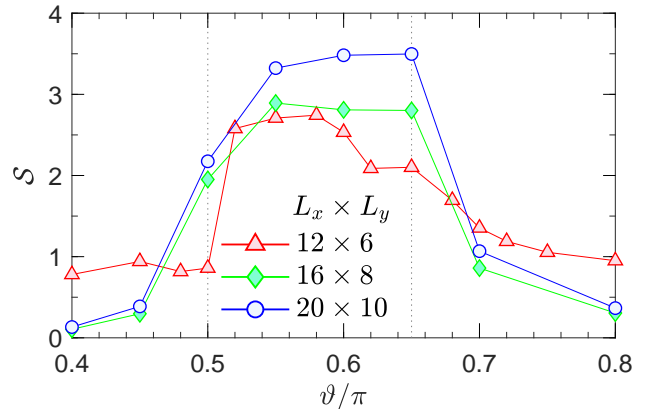


FIG. SM-6: The von Neumann entropy  $\mathcal{S}$  for  $\vartheta/\pi$  ranging from 0.4 to 0.8. The circumferences  $n$  of the clusters are 6 (red triangle), 8 (green diamond), and 10 (blue circle).

## ROLE OF THIRD-NN INTERACTION

Recent *ab initio* calculations on  $\alpha$ -RuCl<sub>3</sub> have highlighted the role played by the third-NN Heisenberg interaction  $J_3 \sum_{\langle\langle\langle i,j \rangle\rangle\rangle} \mathbf{S}_i \cdot \mathbf{S}_j$ . It is shown that even a tiny antiferromagnetic  $J_3$  can enhance the zigzag magnetic order[2]. This physical virtue has already been examined in other theoretical models where competing interactions could lift the degeneracy of the pure  $J_3$  model and give rise to the zigzag order. To verify such conclusions we study the  $\Gamma$ - $J_3$  model to explore the effect of the  $J_3$  term. We find that in the phase diagram the HCTA is indeed adjacent to the zigzag phase but separated by a transition.

Fig. SM-7 shows the evolution of the magnetic orders versus  $J_3$  in a rather wide region. It could be found that the ferromagnetic and antiferromagnetic  $J_3$  model tend to select the FM phase and zigzag phase, respectively, as the ground state with the perturbation of antiferromagnetic  $\Gamma$  term. Between the two, the maximum of  $M_N(\mathbf{Q})$

appears at  $\mathbf{X}$  point of the Brillouin zone (see Fig. 1 of the main text). At  $J_3 = 0$ ,  $M_N(\mathbf{Q})$  at  $\mathbf{M}$  becomes comparable to that at  $\mathbf{X}$ . However, as can be seen from the inset which shows the first derivative of  $M_N(\mathbf{M})$  versus  $J_3$ , the peak locates at a tiny but nonzero  $J_{3,t} \approx 0.075$ . This provides further evidence that the ground state of the HCTA, in which  $J_3$  is zero, is not the zigzag order.

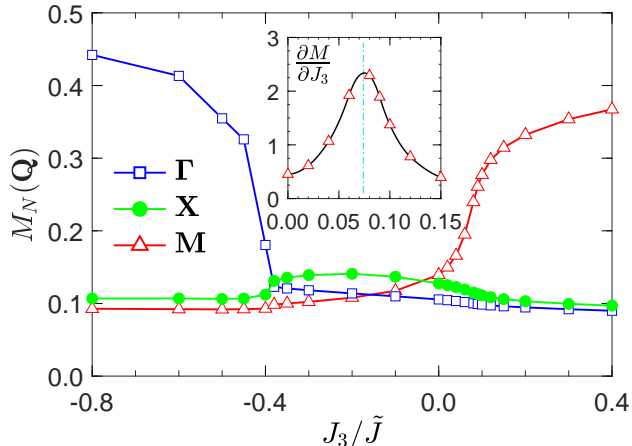


FIG. SM-7: Order parameters  $M_N(\mathbf{Q})$  for the FM order (blue square), X-order (green circle), and zigzag order (red triangle) with  $\mathbf{Q} = \Gamma, \mathbf{X}$ , and  $\mathbf{M}$ , respectively. The circumference  $n$  of the cluster is fixed to be 6. Inset: The first derivative of  $M_N(\mathbf{M})$  versus  $J_3$ .

## IDEAS ON THE LONG CYLINDER

To carry out the DMRG calculations on the long cylinder, there are two apparent issues that should be settled when compared to the traditional DMRG construction. On one hand, proper pinning fields should be applied to the edge spins. To accelerate the convergence as well as to induce meaningful pinning orders, we shall apply pinning fields of order  $\mathcal{O}(1)$  and fix the directions of the three components as they appear in their classical counterparts. On the other hand, the driven interactions should vary with the position, from the left to the right.

In our current model, we fix the interactions at the leftmost and rightmost boundaries, say  $\vartheta_{\min}/\pi = 49/120$  and  $\vartheta_{\max}/\pi = 91/120$ . The interactions inside will vary according to a presupposed protocol, which could be merely the linear rule. Because we only consider the nearest-neighbor interactions  $J$  and  $\Gamma$  along the three bonds, we can distinguish the zigzag ( $\mathbf{X}$  and  $\mathbf{Y}$ ) bonds to the horizontal ( $\mathbf{Z}$ ) bond so as the make the variation of  $\vartheta$  be more smooth. The variation of  $\vartheta$  with position is illustrated in Fig. SM-8, and for each  $\vartheta$ -index shown in the bottom, we have the current value  $\vartheta_x = \vartheta_{\min} + x \cdot \delta\vartheta$  where  $\delta\vartheta = (\vartheta_{\max} - \vartheta_{\min})/[2(L_x - 1)] = 0.005\pi$  in our case. This is to say that there is a  $0.01\pi$  increment for the two successive columns ranging from 0 to  $L_x - 1$ .

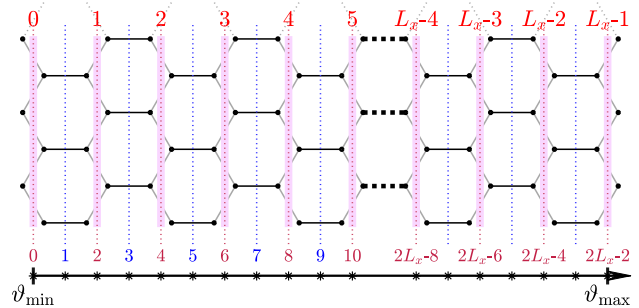


FIG. SM-8: Illustration on the variation of the  $\vartheta$  with position. The series ranging from 0 to  $L_x - 1$  shown in the top denotes the column index. The other series ranging from  $(x =) 0$  to  $2(L_x - 1)$  shown in the bottom denotes the  $\vartheta$ -index. The value of  $\vartheta$  in the vertical dotted line is  $\vartheta_x = \vartheta_{\min} + x \cdot \delta\vartheta$  where  $\delta\vartheta = (\vartheta_{\max} - \vartheta_{\min})/[2(L_x - 1)]$ .

\* zhaojz@lzu.edu.cn

† xiaoqunwang@sjtu.edu.cn

- [1] I. Rousochatzakis and N. B. Perkins, Phys. Rev. Lett. **118**, 147204 (2017).  
 [2] A. Catuneanu, Y. Yamaji, G. Wachtel, Y.-B. Kim, and H.-Y. Kee, npj Quantum Materials **3**, 23 (2018).